

On the Role of Nuclear Motion in Singlet Exciton Fission: The Case of Single-Crystal Pentacene

Alexander Neef,^{*} Mariana Rossi, Martin Wolf, Ralph Ernstorfer, and Hélène Seiler^{*}

Singlet exciton fission (SF), the formation of two triplet excitons from one singlet exciton, involves electronic, nuclear, and spin degrees of freedom as well as their couplings. Despite almost 60 years of research on this process, a complete microscopic understanding is still missing. One important open question concerns the role of nuclear motion in SF. In this perspective, recent results on the exciton dynamics are related to the structural dynamics of single-crystal pentacene and how they provide insights into that open question is shown. To probe the electronic dynamics, orbital-resolved measurements of the electronic structure are carried out using time- and angle-resolved photoemission spectroscopy. With femtosecond electron diffraction and with *ab initio* computations, the complementary nuclear dynamics is tracked. The results from both techniques are summarized, and how they relate to each other is discussed. Then, remaining open questions are outlined and potential routes are identified to tackle them, hopefully guiding future studies.

thus multiplying the excitations. Overall, SF converts a singlet exciton into two independent triplet excitons and thereby connects different spin manifolds. Since the product triplets have opposite spins, the overall spin is conserved and the process spin-allowed. SF occurs in a sequence of steps (Figure 1a). The primary step SF1 is the conversion of a singlet exciton S_1 into a bitriplet exciton (1TT). The bitriplet is thought to separate by triplet hopping^[9] on an ultrafast timescale into the separated bitriplet $^1T \dots T$, we denote this step as SF2. Lastly, the spins of the triplets dephase and two independent triplets form. Despite the early discovery of SF in the 1960s,^[10] there is yet no consensus on a mechanistic theory of SF. The reason is that the initial singlet excitons and final triplet excitons are easy to detect by absorption and emis-

sion, whereas the intermediate states are challenging to observe. Some observations of the intermediate states have been claimed,^[11,12] but a clear picture of their composition and role in SF has yet to emerge.

While there is at least some agreement on the electronic structure of the sequence of intermediate states, the mechanisms connecting them are even more disputed. To get a clear picture, we must distinguish the systems in which SF can occur. SF can either be endothermic as in tetracene or exothermic as in pentacene. It can occur in spatially confined dimers or in quasi-infinite crystals. While the microscopic mechanisms of SF can be expected to widely differ for different SF systems, some general questions are common to all SF systems. A key question is the role of nuclear motion in driving the SF process—that is how are the nuclear and electronic systems coupled to each other. The question is not whether (coherent) nuclear motion occurs, but rather how it affects the SF steps. For SF1, for instance, there are two contrasting views on the role of nuclear motion: 1) SF1 can be accurately described with a frozen lattice approach, in which nuclear motion provides merely an energetic bath. 2) Nuclear motion has to be described explicitly as there might be regions of the potential energy surface in which the coupling between singlet and bitriplet states is greatly enhanced, i.e., conical intersections play a key role. For SF2, the role of nuclear motion is even less understood as this step remains the least probed of all SF steps.

This perspective summarizes recent results on the first two steps of SF in crystalline pentacene (Figure 1c)—a paradigmatic SF material. We tackled the challenge of tracking the SF steps from two sides. First, we used time-resolved and angle-resolved

1. Introduction


Singlet exciton fission (SF) has received much attention in recent years.^[1–8] It is of great physical and technical interest as it is one of the few processes that can controllably split an exciton in half,

A. Neef, M. Wolf, R. Ernstorfer, H. Seiler
Department of Physical Chemistry
Fritz Haber Institute of the Max Planck Society
Faradayweg 4-6, 14195 Berlin, Germany
E-mail: neef@fhi-berlin.mpg.de; helene.seiler@fu-berlin.de

M. Rossi
Max Planck Institute for the Structure and Dynamics of Matter
Luruper Chaussee 149, 22761 Hamburg, Germany

R. Ernstorfer
Institut für Optik und Atomare Physik
Technical University Berlin
Strasse des 17. Juni 135, 10623 Berlin, Germany

H. Seiler
Department of Physics
Freie Universität Berlin
Arnimallee 14, 14195 Berlin, Germany

 The ORCID identification number(s) for the author(s) of this article can be found under <https://doi.org/10.1002/pssa.202300304>.

© 2023 The Authors. *physica status solidi (a) applications and materials science* published by Wiley-VCH GmbH. This is an open access article under the terms of the Creative Commons Attribution License, which permits use, distribution and reproduction in any medium, provided the original work is properly cited.

DOI: 10.1002/pssa.202300304

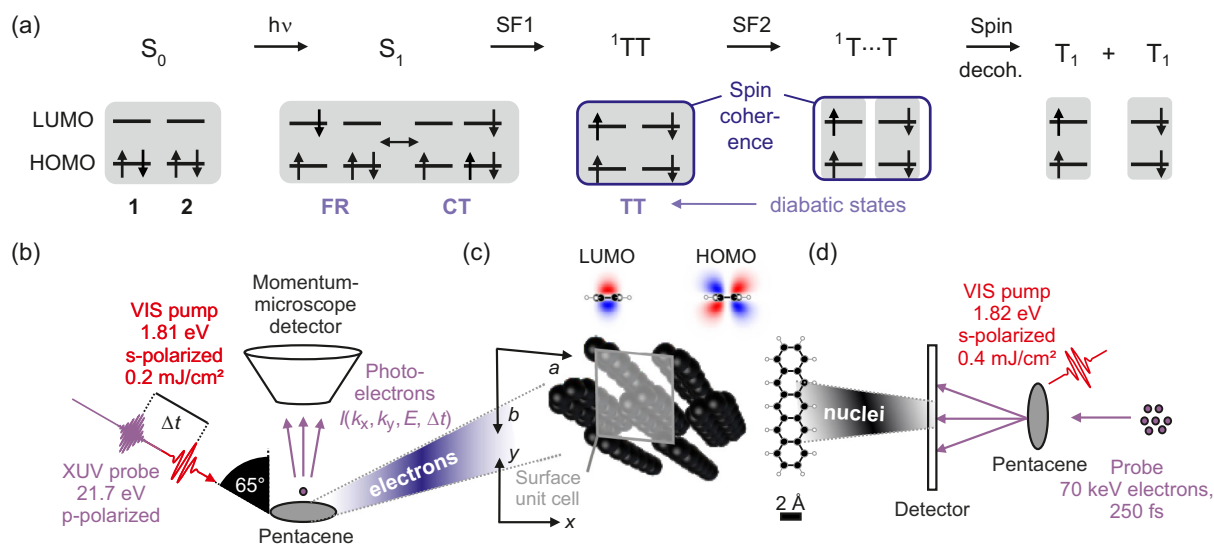


Figure 1. a) Singlet exciton fission (SF) reaction scheme and electronic configurations of the excitonic states. The diabatic configurations refer to a two molecule system with highest-occupied molecular orbital (HOMO) and lowest-unoccupied molecular orbital (LUMO) each. b) Experimental principle of trARPES. c) Crystal structure of pentacene and the structure of the frontier orbitals at the edge of a pentacene molecule. d) Experimental principle of femtosecond electron diffraction. a–c) Reproduced under the terms of the CC BY 4.0 Creative Commons license.^[13] Copyright 2023, The Authors, published by Springer Nature.

photoemission spectroscopy (trARPES) to track the electronic character and dynamics of the excitons (Figure 1b). Second, we followed the nuclear dynamics after the primary step by combining femtosecond electron diffraction (FED, Figure 1d) and ab initio simulations. The combination of these complementary techniques yields a unique view of the complex dynamics of SF, which span electronic and nuclear degrees of freedom, their respective couplings, and several orders of magnitude in time. After introducing the results obtained with each technique, our perspective discusses how these results provide new insights into the role of nuclear motion in SF1 and SF2. We then discuss the remaining open questions and potential routes to tackle them.

2. Electron Dynamics Results

We examined the electronic dynamics with trARPES.^[13] Here, a visible pump pulse populates the lowest bright exciton and an ionizing probe pulse ejects electrons that are collected in a momentum microscope spectrometer. The detector records the in-plane momenta $\mathbf{k} = (k_x, k_y)$ and the kinetic energy E , yielding a 3D photoemission (PE) intensity $I(\mathbf{k}, E)$ for each pump–probe delay Δt . For a more detailed description of the method, see Maklar et al.^[14]

We are interested in the signatures of correlated excited states and expand the PE intensity for different electron configurations i

$$I_i \propto c_i \sum_j S_{ij} M_{ij} \quad (1)$$

where c_i is the coefficient of configuration Φ_i in the total wave function Ψ , S_{ij} is the overlap term between an ionized i and a cationic final state j , and M_{ij} is the orbital-dependent transition matrix

element. The electron correlation in the singlet and bitriplet excitons prohibits casting these states as single electron configurations. Each state will show a main line related to the dominant electron configuration and *satellites* resulting from the admixture of other configurations. The coefficient c_i determines the strength of the peaks in the spectrum (satellite and main lines) and is a measure of the configuration interaction.

The orbital term M_{ij} , in contrast, can—within the plane-wave approximation—be understood as a Fourier transform of the orbital ψ from which an electron was ejected. In the solid state, the electrons reside in Bloch orbitals which may be confined in space. These localized Bloch orbitals $\psi(\mathbf{r}) = \sum_{\mathbf{R}} \phi(\mathbf{r} - \mathbf{R}) F_{\text{env}}(\mathbf{R}) e^{i\mathbf{k} \cdot \mathbf{R}}$ extend over several molecular orbitals ϕ with a localization length λ determined by the envelope function F_{env} . Each factor to ψ is distinctly visible in momentum maps of the PE intensity as shown in Figure 2a. The orbital character is defined by ϕ and leads to a long-range modulation of the PE intensity. The signature of localization is the width $\propto \frac{1}{\lambda}$ of the PE peaks in reciprocal space.

In the experiment, we populate the exciton S_1 with a 1.81 eV visible pump pulse. This leads to two excited peaks: S at 1.81 eV above the valence band maximum (VBM) and X at 0.95 eV above VBM. S can be assigned to the main peak of the singlet exciton and X to a satellite peak. After 500 fs, these signals have transitioned into the lower-energy peak TT at 0.65 eV above VBM, which arises from the bitriplet exciton.

Strikingly, the momentum maps S and TT (Figure 2b) show a very similar intensity pattern—proving the similar lowest-unoccupied molecular orbital (LUMO) character of their parent excitons. Yet, there is a difference: the features in S are much more pronounced than in TT. This translates to a delocalized singlet exciton and a localized bitriplet exciton, thus confirming predictions by theory.^[15] We now turn to the momentum map of X.

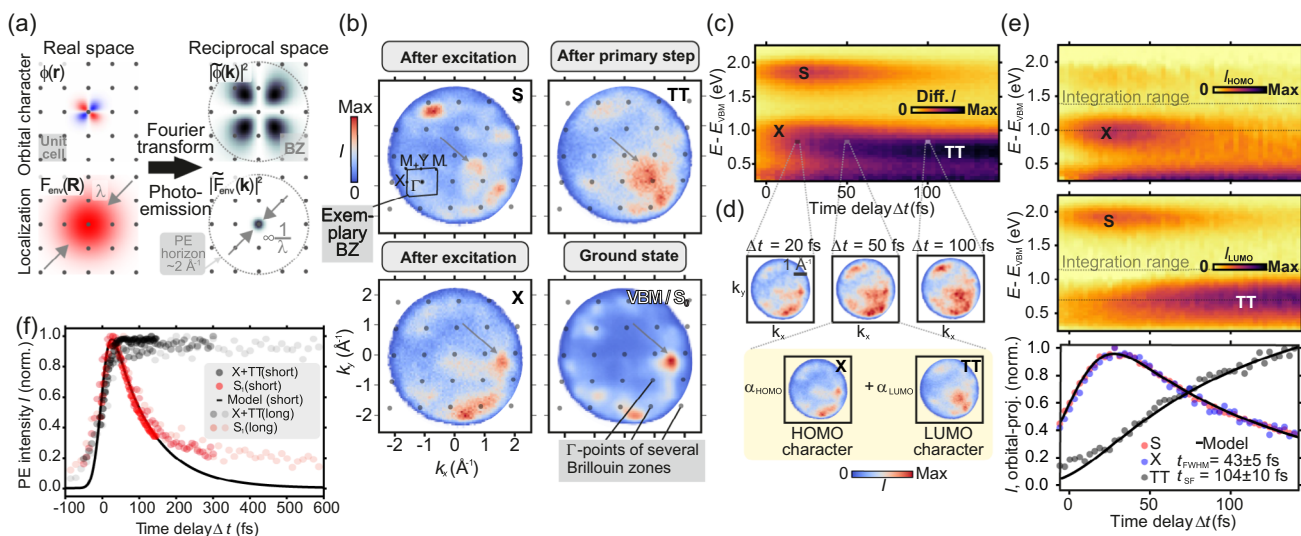


Figure 2. a) PE can be treated as a Fourier transform leading to distinct signatures of the orbital character and the localization of the initial state in momentum maps. b) Momentum maps of the relevant states in SF (S: singlet exciton, TT: bitriplet exciton, X: satellite, VBM: valence band maximum). c) Differential PE intensity (eq. signal subtracted) of the photoexcited states. d) Illustration of the orbital-resolved decomposition. e) Orbital-resolved PE intensity, top HOMO character, and middle LUMO character. The bottom panel shows the energy-integrated signal. f) Dynamics at longer time delays, not orbital resolved. Reproduced under the terms of the CC BY 4.0 Creative Commons license.^[13] Copyright 2023, The Authors, published by Springer Nature.

It looks different from both S and TT and must correspondingly be of different orbital character. However, it shows an intimate similarity with the momentum map of the VBM, and hence X must be of highest-occupied molecular orbital (HOMO) character (the valence band is formed by HOMOs).

The state X is furthermore located at an energy where no electronic state is expected. In contrast, it lies 0.86 eV below S_1 , which is the energy of an individual triplet exciton in pentacene. This suggests that it might be a transition from the singlet exciton state to an excited cation, which differs from the ground state of the cation yielding signal S by a triplet excitation. By analyzing the possible transitions, we have shown that indeed this is the case and that X is a *satellite* peak of the singlet exciton and arises from an admixture of charge-transfer (CT) states into the singlet exciton. The equal strengths of the S and X peaks indicate that S_1 is roughly a 1:1 mixture of Frenkel and CT configurations.

We used the momentum maps of X and TT to decompose the SF dynamics based on the orbital character of the signal (Figure 2c,d). The results unveil that what could be assumed to be the energetic relaxation of a lower energy state is the signal from two energetically overlapping signals, the CT satellite of S_1 and the main peak of 1TT (Figure 2e). The separation of the signals allowed us to obtain clean, orbital-projected dynamics for signal with HOMO and LUMO character. The orbital-projected signals S (with LUMO character) and X (with HOMO character) show the same dynamics and can be fitted together with signal TT (with LUMO character) as product state in a model with a single time constant. These results clearly show that 1TT is formed by the decay of S_1 with a $t_{SF} = 104 \pm 10$ fs time constant. If there is any population of states with diabatic bitriplet character by optical excitation, it is only marginal. Together with the large CT character in S_1 , this is strong evidence for the CT-mediated mechanism in the solid state,^[13] adding to the evidence found

for state mixing of the singlet exciton in polymers^[16] and in solution.^[17]

After the decay of the singlet exciton, slower dynamics kick in (Figure 2f). A second exponential decay with a slower ≈ 600 fs time constant becomes visible. Furthermore, there is an energetic relaxation of S by ≈ 50 meV over the course of the first 150 fs (Figure S1a, Supporting Information). These observations put together suggest that after ≈ 200 fs, S no longer originates from S_1 but from a different state. The only other state that could yield this signal is 1TT , provided it has a significant CT character. The late S is then a CT satellite of the bitriplet exciton and the second timescale we observe thus concerns the decay of 1TT and SF2. In this step, $^1T \dots T$ is formed, which has no CT character, and thus features no CT satellite in the PE signal. The reason why we don't see a change in the TT signal is that the two different bitriplet species are almost isoenergetic. Nonetheless, there is a small upshift in TT by ≈ 10 meV in the time window 200 to 2000 fs (Figure 1b, Supporting Information). This might be a further indication of the loss of the stabilizing CT character when going from 1TT to $^1T \dots T$.

3. Nuclear Dynamics Results

The importance of atomic structure and nuclear dynamics in determining SF properties (e.g., rate, yield) has been reported in numerous studies.^[8,12,18–20] Yet, just like an orbital-resolved view of SF had been lacking, direct experimental observations of the structural dynamics involved in SF on the relevant timescales have also remained elusive. Time-resolved Raman spectroscopies were successfully employed to reveal structural dynamics at the femtosecond timescale, but they are restricted to local molecular changes.^[21,22] Several time-resolved optical

spectroscopy studies also reported on coherent phonon dynamics in SF systems.^[8,20,23] However, there is no a priori reason why atomic motion involved in SF should be purely coherent or purely incoherent.^[24] Time-resolved diffraction techniques using X-rays or electrons can access both coherent and incoherent nuclear motion. Such techniques can probe the dynamics of structural changes in crystals with unit cell sizes up to several hundred atoms.^[25,26] Diffraction-based techniques are therefore uniquely poised to reveal the intermolecular and collective nuclear motion that may be involved in SF. Such collective motion involving several molecules have been predicted to drastically affect transport properties,^[27–29] and can be expected to have a large impact on the SF process as well (e.g., via a modification of the π - π overlap in two adjacent acenes).

To complement the electronic dynamics measurements described earlier, we have carried out FED experiments on the

same pentacene crystals. These complementary experiments have enabled us to directly access the nuclear dynamics accompanying the SF process in real time, thereby yielding insights on the role of nuclear motion in SF. While the trARPES measurements focused on SF1, our FED measurements focus on SF2. As we shall see, rich structural dynamics accompanies SF2 in crystalline pentacene on the picosecond timescale. A schematic illustration of the experiment is shown in Figure 1d, and an exemplary diffraction of the pentacene crystals is shown in Figure 3a. A detailed description of the method is given in ref. [30]. The pentacene samples investigated with FED are 30–80 nm thick, free-standing single-crystalline films excited with a 50 fs visible pump pulse resonant with the lowest bright exciton, i.e., the optical excitation in both types of experiments is equivalent. The nuclear dynamics are probed with a femtosecond bunch of electrons diffracting off the nonequilibrium lattice and

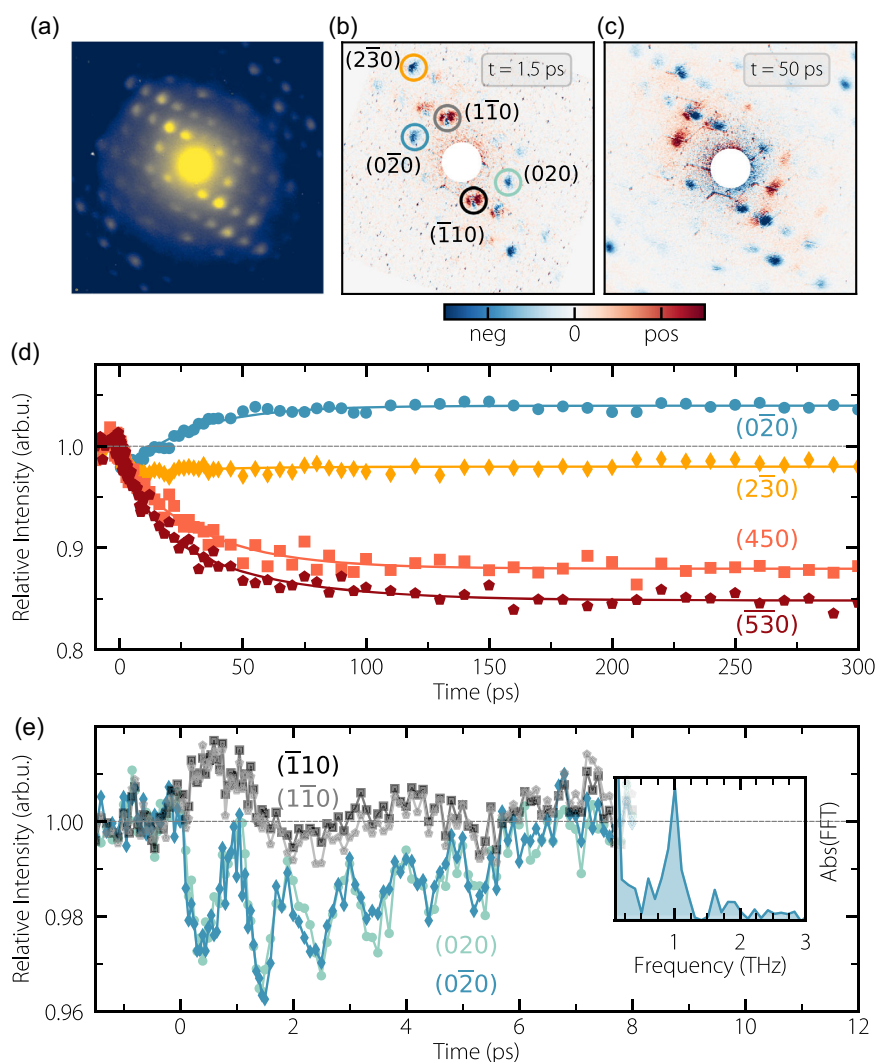


Figure 3. a) Equilibrium electron diffraction pattern of a 50 nm thin slab of single-crystal pentacene. b) Difference between the diffraction pattern at $t = 1.5$ ps after photoexcitation and before photoexcitation. c) Same as in (b) but at $t = 50$ ps. d) Time-resolved diffraction intensities for certain Bragg peaks. Plain lines are biexponential fits to data points (markers). e) A zoom in the first 10 ps of the dynamics reveals pronounced oscillations at 1 THz of certain Bragg peaks. Reproduced under the terms of the CC BY 4.0 Creative Commons license.^[31] Copyright 2021, The Authors, some rights reserved; exclusive licensee American Association for the Advancement of Science.

diffraction patterns are collected by a detector for each pump-probe delay Δt . The temporal resolution of the FED experiment is 250 fs.

The FED experiments resulted in three main observations: 1) incoherent nuclear dynamics with a time constant of 1.6 ps, 2) the buildup of a structural distortion with a timescale of around 30 ps, 3) and pronounced coherent nuclear motion at 1 THz in some Bragg peaks. We have assigned the 1.6 ps time constant to the reorganization of the crystal lattice resulting from the change in potential energy surface caused by SF1. Such reorganization processes are ubiquitous in physical chemistry and their observation is part of a comprehensive understanding of the SF steps. The second time constant of 30 ps relates to the buildup of a structural distortion. As can be seen in Figure 3b–d, some Bragg peak intensities evolve to positive values on that timescale. In ref. [31], we discuss how such signals cannot reflect thermal heating effects and must arise from a light-induced lattice distortion. We assigned the slower time constant to the spatial separation of the triplets via triplet hopping. Our physical picture is that the electronically independent triplets remain spatially close right after the disintegration of 1T_1 , and that they spatially diffuse away from each other over tens of picoseconds until a spatially homogeneous distribution of triplets is achieved after $\Delta t \approx 50$ ps. The electronically independent triplets form exciton–polarons, and the observed structural distortion

reflects their lattice signature. An interesting consequence of that picture is that $^1T_1 \dots T_1$ is not a single state, but rather dynamically evolves as the triplets spatially separate.

In addition to the incoherent nuclear motion, we observed coherent oscillations of several Bragg peaks at the frequency of 1 THz, with a dephasing time of around 4 ps. The question of whether this motion facilitates or merely accompanies the subsequent steps of SF then naturally arises. To answer that question, it is essential to identify the real-space motions at the origin of the coherent structural dynamics. This can be done partly with structure factor analysis. Due to the complexity of the pentacene crystal, however, an identification of the motions can only be obtained with complementary theoretical work.

We performed ab initio Ehrenfest dynamics including a laser excitation with real-time time-dependent density-functional theory (RT-TDDFT) for a total simulation time of 50 fs, as well as molecular dynamics (MD) simulations on large unit cells of crystalline pentacene with an empirical force field for several picoseconds. Technical details about the simulations are extensively discussed in ref. [31]. As shown in **Figure 4a**, shortly after an excitation with a laser pulse polarized at the same crystal direction as in the experiment and with a similar energy, one can follow the movement of the pentacene molecules. When projecting the molecular motion on the normal modes of the pentacene crystal unit cell, we observe that the motion is dominated by

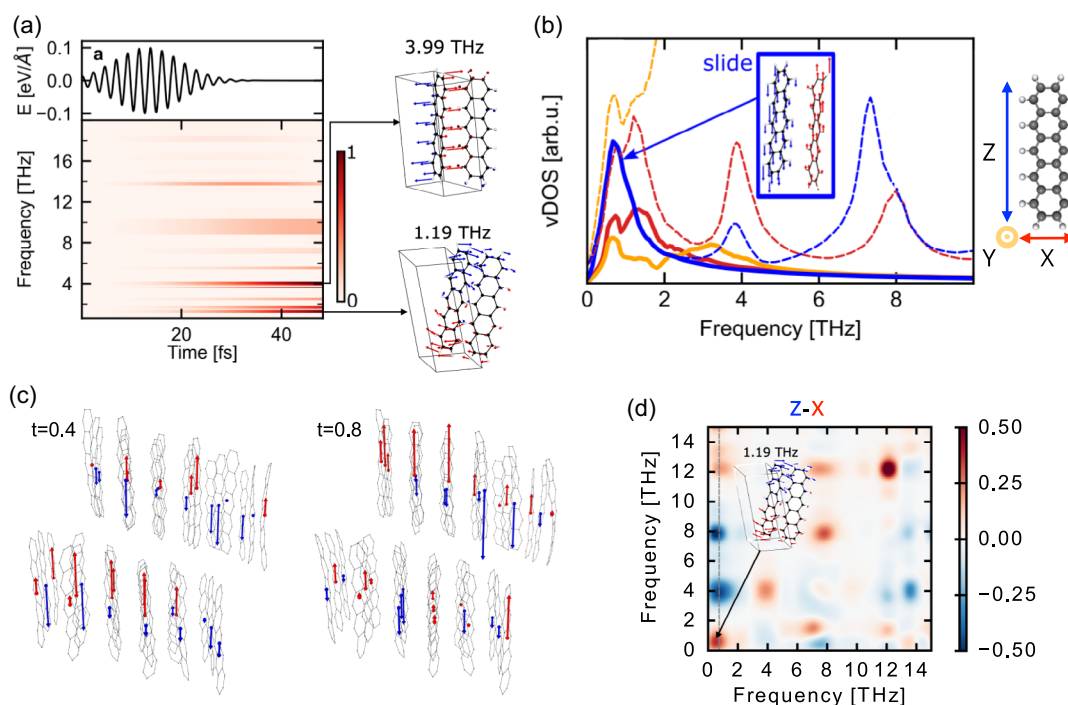


Figure 4. a) Projection of atomic displacements on the vibrational normal modes of the pentacene crystal, during Ehrenfest dynamics with a laser excitation as shown in the top panel (real-time time-dependent density-functional theory [RT-TDDFT]). Color code indicates the relative magnitudes, at each time step, of each normal mode coefficient. The harmonic frequencies of each mode are shown on the y axis. Relevant normal modes are shown explicitly. b) Partial equilibrium vibrational density of states (vDOS) projected onto the X, Y, and Z axes defined in the inset. Dashed lines represent data obtained for carbon atoms only and solid lines for the molecular center of mass (CM). c) Exemplary MD snapshots showing the whole simulation cell ($3 \times 6 \times 2$ molecules). The velocity vectors of molecular CM along Z are indicated as the red and blue arrows. d) The 2D-vDOS correlation plot extracted from MD simulations when accounting for the atomic motion projected on the Z and X axes defined in panel (b). Reproduced under the terms of the CC BY 4.0 Creative Commons license.^[31] Copyright 2021, The Authors, some rights reserved; exclusive licensee American Association for the Advancement of Science.

intra- and intermolecular modes below 16 THz, and in particular intermolecular modes along the short and normal axis of the molecules. When analyzing equilibrium and nonequilibrium long-time MD in a $3 \times 3 \times 2$ pentacene crystal supercell, we concluded that incoherent excitations of modes at around 1 THz in the crystal lead to oscillations in the 020 and 0 $\bar{2}$ 0 Bragg peaks similar to those observed in experiment (see ref. [31]) and that projecting the vibrational density of states (vDOS) on the long axis of the molecules show a pronounced density of vibrational states connected to sliding motions around 1 THz. Overall, these motions are dominated by out-of-phase sliding of neighboring pentacene units, as shown in Figure 4c. Finally, by building and analyzing 2D correlation plots of the vDOS, we find strong indication that the sliding motions along the long axis couple to modes along the other two axes that were populated in the RT-TDDFT Ehrenfest dynamics. An example is shown in Figure 4d. To conclude, the simulations indicate activated motion along the long axis that might assist SF2, after the initial electron–phonon coupling that populates specific nuclear motions following photoexcitation and SF1.

4. Discussion and Open Questions

The trARPES data clearly establish the electronic mechanism of SF1 in pentacene. With this result at hand, we turn to the role of

nuclear motion in SF1 apart from providing an energetic bath to take up excess energy.

Several theoretical^[32,33] and 2D spectroscopy^[8,20,23,34] works have emphasized the importance of the consistently observed nuclear coherence. If a specific nuclear geometry with an enhanced coupling between electrons and nuclei or a geometry with reduced energetic separation of the states is important, one expects a faster SF1 rate at this position. The rate would in effect oscillate with the period of the phonon shuttling the nuclear wave packet to that position. However, we see no signs of oscillatory features in the decay dynamics of S_1 within the frequency range < 20 THz that our time resolution allows.

In agreement with theoretical works that employ an incoherent phonon bath,^[6,35] we hence interpret the coherent molecular vibrations that occur < 100 fs as modes that take up the surplus energy of the optical transition, but that do not act back on the SF1 dynamics (see Figure 5). Furthermore, while our trARPES measurement cannot directly determine the influence of incoherent nuclear dynamics on SF1, the involvement of CT states that are close to degenerate with Frenkel states has implications for nuclear motion. CT states lead to a delocalization of the singlet exciton over several molecules, thereby reducing the reorganization energy and the extent of nuclear motion involved with SF1 as each molecule only feels a fractional charge.^[36]

We now focus on SF2. Timescales of the formation of $^1T \dots T$ have been estimated to be 1.3–1.8 ps in

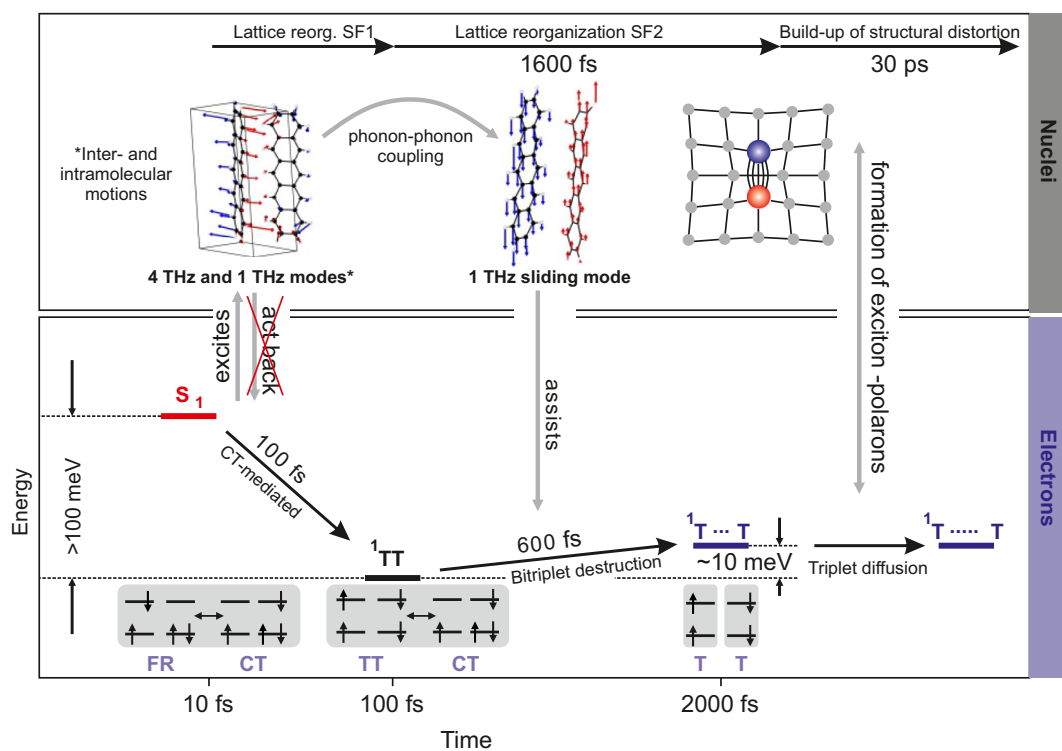


Figure 5. Overview of the nuclear and electronic dynamics in the first two steps of SF in crystalline pentacene. S_1 decays via a charge-transfer (CT)-mediated mechanism to the > 100 meV lower 1TT , accompanied by inter- and intramolecular vibrations that take up the excess energy. This dark state then loses its stabilizing CT character to form the dark $^1T \dots T$ via triplet hopping. The observed 1 THz phonon might assist this process by significantly changing the electronic coupling between adjacent pentacene molecules. On later timescales, a structural distortion builds up, flagging the formation of triplet exciton–polarons, while the spin-correlated triplets diffuse further.

pentacene^[37,38] and 2 ps in 6,13-bis(triisopropyl-silylethynyl) (TIPS) pentacene.^[12] These timescales are on the same order of magnitude as the 600 fs time constant that we observe in the trARPES measurements. However, the timescales observed with transient absorption might also indicate lattice reorganization as discussed later.

Our FED measurements provide direct insights into the lattice dynamics of SF2. They demonstrate the joint presence of incoherent and coherent atomic motions during that step. The incoherent time constant of 1.6 ps which we have observed in the Bragg peak dynamics can be attributed to the lattice reorganization energy, which follows changes in the potential energy surface resulting from SF1. Simultaneously with this decay, the nuclei oscillate with 1 THz. Combining structure factor analysis and theory, we showed that this movement mostly changes the long axis offset of adjacent pentacene molecules. In the PE data, we do not see an effect of this motion, because it only leads to an additional disorder in the transfer integrals and therefore an energetic broadening of the states—which is hard to disentangle from other effects. Coming back to the interplay of nuclear and electron dynamics, we focus on the possible effect of the 1 THz phonon on SF2. Electronically, ¹TT might lose its stabilizing CT character by triplet hopping^[9,39,40] or by a loss of CT character within a dimer. Both are controlled by a product of the intermolecular electronic couplings of HOMO and LUMO. The 1 THz phonon has a strong effect on these couplings and might thereby assist the transition from ¹TT to ¹T . . . T. If the coupling between the long axis motion and the triplet-hopping rate is strong enough, we expect to see a coherent modulation of the SF2 rate.

We close this perspective with some open questions. The main question to tackle, in our opinion, is to shed light on the electronic mechanisms involved in SF2. This step, which has been much less investigated compared to SF1, is nevertheless of crucial importance for applications. Indeed, the chemical species of relevance for SF-based photovoltaic applications is not the intermediate bitriplet ¹TT formed after SF1, but rather the fully independent triplet excitons. Since high temporal resolution is not required to observe the electronic dynamics of SF2, trARPES with high energy resolution (10 meV would be needed in pentacene) could potentially be employed to separate ¹TT and ¹T . . . T based on their energies. While the momentum maps of both species look similar, a trARPES study with a larger signal in the excited states might reveal subtle differences that trace back to the CT character of ¹TT and even allow a projection of the signal onto different orbital characters. Alternatively, one should study SF2 in different acenes with favorable energetics. For instance, in tetracene, ¹TT and ¹T . . . T are separated by > 50 meV and might be isolated more easily in trARPES measurements with sufficient energy resolution.^[39] Furthermore, ¹TT and S₁ have a large energy offset in hexacene such that it should be possible to distinguish these two states more easily.^[41]

Having direct access to the nuclear dynamics involved in SF1 using diffraction-based techniques will provide an even more comprehensive picture of SF1. It may reveal incoherent lattice dynamics involved in SF1, as well as coherent motions of high-frequency phonons that cannot currently be resolved. Results from theory—for instance indicating phonon–phonon

coupling between 1 THz and 4 or 8 THz modes—could be directly compared with experiments. Reaching the necessary temporal resolution to observe SF1 with FED instruments comes into technical reach thanks to electron pulse compression techniques and relativistic mega electron volt electron diffractometers.^[42] Investigating SF1 with trARPES and a time resolution of ≈20 fs could further assess the role of high-frequency vibrations.

Another interesting direction is directly probing the electron–phonon coupling by exciting specific phonons. An earlier study has observed an increase in triplet exciton yield by photoexciting tetracene crystals with pulse trains separated by the oscillation period (500 fs) of an intermolecular vibration.^[43] With a pump–pump–probe experiment, it should be possible to coherently control different SF steps (for some examples of coherent control, see refs. [44,45]). Such an experiment would allow a more direct assessment of the role of specific vibrations in the SF process.

Furthermore, the mechanism and the role of nuclear motion in endothermic SF need further investigation. In tetracene, the energies of the two product triplet excitons sum to 200 meV more energy than the initial singlet exciton, making it useful for photovoltaic applications. An increase in entropy is necessary to drive this process uphill. The progress on this question has been reviewed,^[46] but some questions remain, specifically regarding the microscopic mechanism. The endothermicity of the individual steps (as opposed to the energy difference between singlets and two triplets) remains to be determined reliably. Future diffraction studies might reveal the vibrational modes that provide the required energy and observe a cooling of the lattice. Finally, there is a lack of theoretical work on the microscopic mechanism that might then reveal insights on the limits to endothermicity.

Theoretical methods are also necessary to fully characterize and understand the several steps of SF in pentacene. Much progress has been made with model Hamiltonians and the combination of several different simulation techniques,^[2,47] which have provided plausible scenarios of the full SF process, and ruled out many others. However, a full quantum and atomistic understanding of all steps related to the SF process in pentacene remains elusive. One of the main current open challenges lies on the quality of the electronic–structure theory that can be applied to realistic systems,^[19] in particular describing double excitations in periodic systems.^[48] Ideally, methods like time-dependent coupled cluster could capture the SF process accurately, but their computational burden has so far been prohibitive for applications in large crystalline unit cells. In addition, the experimental work presented here makes it clear that one also needs a methodology able to capture nonadiabatic electron–phonon coupling with quantum nuclear dynamics at long timescales, especially to fully unravel SF2. This surpasses the realm of applicability of methods like “vanilla” Ehrenfest dynamics and calls for others, which are either not accurate or prohibitive due to their cost.^[49] There is certainly a lot of space for theoretical developments in this area.

This perspective has shown how the combination of complementary experimental and theoretical techniques yields new insights into the SF process in pentacene. We have focused here on the role of nuclear motion, and shown that while nuclear motion may not drive SF1, it may play an important role in

SF2. We have also identified open questions, which we hope will be useful to guide future studies on the process. Overall, we expect that future progress in our understanding of SF will lead to further refinements in the steps and mechanisms at play.^[50] Tackling these open questions will go hand in hand with methodological improvements both from the experimental and theoretical sides.

Supporting Information

Supporting Information is available from the Wiley Online Library or from the author.

Acknowledgements

This work was funded by the Deutsche Forschungsgemeinschaft (DFG)—Projekt Nummer 182087777—SFB 951 (B17 and A13), the Max Planck Society, and the European Research Council (ERC) under the European Union's Horizon 2020 research and innovation program (grant agreement no. ERC-2015-CoG-682843). H.Se. acknowledges support from the Swiss National Science Foundation under grant no. P2SKP_2184100. [Correction added after publication 10 January 2024: The affiliation of the author M. Rossi has been corrected.]

Open Access funding enabled and organized by Projekt DEAL.

Conflict of Interest

The authors declare no conflict of interest.

Keywords

ab initio computations, femtosecond electron diffraction, organic crystals, singlet exciton fission, time- and angle-resolved photoemission spectroscopy

Received: April 18, 2023

Revised: June 6, 2023

Published online: July 14, 2023

- [1] M. C. Hanna, A. J. Nozik, *J. Appl. Phys.* **2006**, *100*, 074510.
- [2] M. B. Smith, J. Michl, *Chem. Rev.* **2010**, *110*, 6891.
- [3] W.-L. Chan, M. Ligges, A. Jailaubekov, L. Kaake, L. Miaja-Avila, X.-Y. Zhu, *Science* **2011**, *334*, 1541.
- [4] D. N. Congreve, J. Lee, N. J. Thompson, E. Hontz, S. R. Yost, P. D. Reuswig, M. E. Bahlke, S. Reineke, T. Van Voorhis, M. A. Baldo, *Science* **2013**, *340*, 334.
- [5] S. R. Yost, J. Lee, M. W. B. Wilson, T. Wu, D. P. McMahon, R. R. Parkhurst, N. J. Thompson, D. N. Congreve, A. Rao, K. Johnson, M. Y. Sfeir, M. G. Bawendi, T. M. Swager, R. H. Friend, M. A. Baldo, T. Van Voorhis, *Nat. Chem.* **2014**, *6*, 492.
- [6] T. C. Berkelbach, M. S. Hybertsen, D. R. Reichman, *J. Chem. Phys.* **2014**, *141*, 074705.
- [7] M. Einzinger, T. Wu, J. F. Kompalla, H. L. Smith, C. F. Parkinson, L. Nienhaus, S. Wiegold, D. N. Congreve, A. Kahn, M. G. Bawendi, M. A. Baldo, *Nature* **2019**, *571*, 90.
- [8] H.-G. Duan, A. Jha, X. Li, V. Tiwari, H. Ye, P. K. Nayak, X.-L. Zhu, Z. Li, T. J. Martinez, M. Thorwart, R. J. D. Miller, *Sci. Adv.* **2020**, *6*, eabb0052.
- [9] G. D. Scholes, *J. Phys. Chem. A* **2015**, *119*, 12699.
- [10] C. E. Swenberg, W. T. Stacy, *Chem. Phys. Lett.* **1968**, *2*, 327.
- [11] H. L. Stern, A. J. Musser, S. Gelinias, P. Parkinson, L. M. Herz, M. J. Bruzek, J. Anthony, R. H. Friend, B. J. Walker, *Proc. Natl. Acad. Sci. U.S.A.* **2015**, *112*, 7656.
- [12] R. D. Pensack, E. E. Ostroumov, A. J. Tilley, S. Mazza, C. Grieco, K. J. Thorley, J. B. Asbury, D. S. Seferos, J. E. Anthony, G. D. Scholes, *J. Phys. Chem. Lett.* **2016**, *7*, 2370.
- [13] A. Neef, S. Beaulieu, S. Hammer, S. Dong, J. Maklar, T. Pincelli, R. P. Xian, M. Wolf, L. Rettig, J. Pflaum, R. Ernstorfer, *Nature* **2023**, *616*, 275.
- [14] J. Maklar, S. Dong, S. Beaulieu, T. Pincelli, M. Dendzik, Y. W. Windsor, R. P. Xian, M. Wolf, R. Ernstorfer, L. Rettig, *Rev. Sci. Instrum.* **2020**, *91*, 123112.
- [15] S. Sharifzadeh, P. Darancet, L. Kronik, J. B. Neaton, *J. Phys. Chem. Lett.* **2013**, *4*, 2197.
- [16] D. E. Mccooy, T. Feo, T. A. Harvey, R. O. Prum, *Nat. Commun.* **2018**, *9*, article no. 2999.
- [17] E. A. Margulies, C. E. Miller, Y. Wu, L. Ma, G. C. Schatz, R. M. Young, M. R. Wasielewski, *Nat. Chem.* **2016**, *8*, 1120.
- [18] K. Kolata, T. Breuer, G. Witte, S. Chatterjee, *ACS Nano* **2014**, *8*, 7377.
- [19] S. M. Janke, M. Rossi, S. V. Levchenko, S. Kokott, M. Scheffler, V. Blum, *Electron. Struct.* **2020**, *2*, 035002.
- [20] A. A. Bakulin, S. E. Morgan, T. B. Kehoe, M. W. B. Wilson, A. W. Chin, D. Zigmantas, D. Egorova, A. Rao, *Nat. Chem.* **2016**, *8*, 16.
- [21] S. M. Hart, W. R. Silva, R. R. Frontiera, *Chem. Sci.* **2018**, *9*, 1242.
- [22] C. Schnedermann, A. M. Alvertis, T. Wende, S. Lukman, J. Feng, F. A. Y. N. Schröder, D. H. P. Turban, J. Wu, N. D. M. Hine, N. C. Greenham, A. W. Chin, A. Rao, P. Kukura, A. J. Musser, *Nat. Commun.* **2019**, *10*.
- [23] K. Miyata, Y. Kurashige, K. Watanabe, T. Sugimoto, S. Takahashi, S. Tanaka, J. Takeya, T. Yanai, Y. Matsumoto, *Nat. Chem.* **2017**, *9*, 983.
- [24] A. M. Alvertis, S. Lukman, T. J. H. Hele, E. G. Fuemmeler, J. Feng, J. Wu, N. C. Greenham, A. W. Chin, A. J. Musser, *J. Am. Chem. Soc.* **2019**, *141*, 17558.
- [25] M. Gao, C. Lu, H. Jean-Ruel, L. C. Liu, A. Marx, K. Onda, S.-y. Koshihara, Y. Nakano, X. Shao, T. Hiramatsu, G. Saito, H. Yamochi, R. R. Cooney, G. Moriena, G. Sciaini, R. J. D. Miller, *Nature* **2013**, *496*, 343.
- [26] E. Collet, M.-H. Lemeé-Cailleau, M. Buron-Le Cointe, H. Cailleau, M. Wulff, T. Luty, S.-Y. Koshihara, M. Meyer, L. Toupet, P. Rabiller, S. Techert, *Science* **2003**, *300*, 612.
- [27] J. Aragón, A. Troisi, *Phys. Rev. Lett.* **2015**, *114*.
- [28] A. S. Eggeman, S. Illig, A. Troisi, H. Sirringhaus, P. A. Midgley, *Nat. Mater.* **2013**, *12*, 1045.
- [29] G. Schweicher, G. D'avino, M. T. Ruggiero, D. J. Harkin, K. Broch, D. Venkateshvaran, G. Liu, A. Richard, C. Ruzié, J. Armstrong, A. R. Kennedy, K. Shankland, K. Takimiya, Y. H. Geerts, J. A. Zeitler, S. Fratini, H. Sirringhaus, *Adv. Mater.* **2019**, *31*, 1902407.
- [30] L. Waldecker, R. Bertoni, R. Ernstorfer, *J. Appl. Phys.* **2015**, *117*, 044903.
- [31] H. Seiler, M. Krynski, D. Zahn, S. Hammer, Y. W. Windsor, T. Vasileiadis, J. Pflaum, R. Ernstorfer, M. Rossi, H. Schwoerer, *Sci. Adv.* **2021**, *7*, eabg0869.
- [32] P. M. Zimmerman, C. B. Musgrave, M. Head-Gordon, *Acc. Chem. Res.* **2013**, *46*, 1339.
- [33] H. Tamura, M. Huix-Rotllant, I. Burghardt, Y. Olivier, D. Beljonne, *Phys. Rev. Lett.* **2015**, *115*, 107401.
- [34] A. J. Musser, M. Liebel, C. Schnedermann, T. Wende, T. B. Kehoe, A. Rao, P. Kukura, *Nat. Phys.* **2015**, *11*, 352.
- [35] S. Refaely-Abramson, F. H. Da Jornada, S. G. Louie, J. B. Neaton, *Phys. Rev. Lett.* **2017**, *119*, 267401.
- [36] A. Devos, M. Lannoo, *Phys. Rev. B* **1998**, *58*, 8236.

- [37] A. R. S. Kandada, A. Petrozza, G. Lanzani, *Phys. Rev. B* **2014**, *90*, 075310.
- [38] T. S. Lee, Y. L. Lin, H. Kim, B. P. Rand, G. D. Scholes, *Can. J. Chem.* **2019**, *97*, 465.
- [39] C. K. Yong, A. J. Musser, S. L. Bayliss, S. Lukman, H. Tamura, O. Bubnova, R. K. Hallani, A. Meneau, R. Resel, M. Maruyama, S. Hotta, L. M. Herz, D. Beljonne, J. E. Anthony, J. Clark, H. Sirringhaus, *Nat. Commun.* **2017**, *8*, 1.
- [40] A. J. Musser, J. Clark, *Annu. Rev. Phys. Chem* **2019**, *70*, 323.
- [41] K. Miyata, F. S. Conrad-Burton, F. L. Geyer, X.-Y. Zhu, *Chem. Rev.* **2019**, *119*, 4261.
- [42] D. Ehberger, K. J. Mohler, T. Vasileiadis, R. Ernstorfer, L. Waldecker, P. Baum, *Phys. Rev. Appl.* **2019**, *11*.
- [43] E. M. Grumstrup, J. C. Johnson, N. H. Damrauer, *Phys. Rev. Lett.* **2010**, *105*, 257403.
- [44] J. G. Horstmann, H. Böckmann, B. Wit, F. Kurtz, G. Storeck, C. Ropers, *Nature* **2020**, *583*, 232.
- [45] Maklar, J. et al. Coherent Light Control of a Metastable Hidden Phase. arXiv: 2206.03788, **2022**.
- [46] D. Casanova, *Chem. Rev.* **2018**, *118*, 7164.
- [47] T. C. Berkelbach, M. S. Hybertsen, D. R. Reichman, *J. Chem. Phys.* **2013**, *138*, 114102.
- [48] A. M. Lewis, T. C. Berkelbach, *J. Phys. Chem. Lett.* **2020**, *11*, 2241.
- [49] E. S. Gil, G. Granucci, M. Persico, *J. Chem. Theory Comput.* **2021**, *17*, 7373.
- [50] A. J. Musser, H. Stern, *Nature* **2023**, *616*, 255.